Journal of Materials Chemistry A

Accepted Manuscript

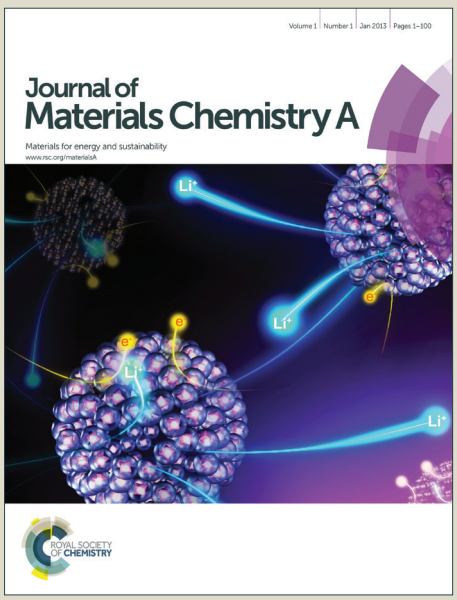

ROYAL SOCIETY OF CHEMISTRY

www.rsc.org/materialsA

Vertically Oriented MoS_2 and WS_2 Nanosheets Directly Grown on Carbon Cloth as Efficient and Stable 3-Dimensional Hydrogen-Evolving Cathode

Ya Yan [a], BaoYu Xia [a], Nan Li [a], Zhichuan Xu [b], Adrian Fisher [c], Xin Wang [a]*

[a] School of Chemical and Biomedical Engineering, Nanyang Technological University, 50 Nanyang Avenue, 639798 Singapore

[b] School of Materials Science and Engineering, Nanyang Technological University, Singapore 639798, Singapore.

[c] Department of Chemical Engineering and Biotechnology, University of Cambridge, New Museums Site, Pembroke Street, Cambridge, CB2 3RA, UK

* Corresponding author. E-mail: WangXin@ntu.edu.sg; Fax: +65 67947553.

Abstract

Development of non-noble-metal based hydrogen-evolving catalysts is essential to practical application of water-splitting devices. Improvement of both the activity and stability of such catalysts remains a key challenge. In this work, a simple solvothermal method is developed to directly grow MoS_2 and WS_2 on carbon cloth with vertically oriented nanosheet layers. With the unique layer orientation that maximally exposes active edge sites as well as a rapid release of small gas bubbles to maintain large working area, such prepared 3-dimensional electrodes exhibit high activity towards HER. In the meantime, they also exhibit prominent electrochemical durability thanks to the strong bonding between the nanosheet layers and the substrate along with the self-removal of the as-formed H_2 bubbles from the nano-porous electrode surface.

Hydrogen generation through water electrolysis has being extensively investigated as an attractive way to store energy from renewable sources.[1, 2] The most effective electrocatalytic materials for the hydrogen evolution reaction (HER) are Pt group metals, but their high cost and scarcity limits the widespread use.[3] As such, developing efficient and inexpensive HER catalysts with high stability are highly desirable but remain challenging. By far, both theoretical and experimental studies have highlighted the great promise of layered transitional-metal dichalcogenides (LTMDs), such as molybdenum disulfide (MoS_2) and its derivatives, as efficient and low cost catalysts for hydrogen evolution.[4-7] Tungsten disulfide (WS_2) has an analogous structure to MoS_2 and these compounds share similar physical and chemical properties. Thus WS_2 has also received some attention as an electrocatalyst for HER for almost 20 years.[8-11]

Since the edges of MoS_2 were identified as active sites for HER,[12] a lot of research efforts have been focused on the growth of MoS_2/WS_2 nanostructures that maximally expose active edge sites for large-scale application.[13-16] Previously, Cui et al. first demonstrated thin film structured HER electrode with vertically aligned MoS_2 molecular layers grown on flat substrates.[17] Later, the same approach was extended to the growth of $MoSe_2$ on rough and curved surfaces in an attempt to increase the exposed edges,[18] as the number of the exposed edge sites is still limited on the flat substrates. Unfortunately, the fabrication process of the nanostructured HER electrodes is rather complicated and also difficult to control. Recently, Jiang et al. successfully demonstrated the construction of vertically aligned MoS_2 nanoplatelets electrode with a "superaerophobic" surface, which allows efficient removal of gas bubbles and ensures high electrochemical activity. [13] Unfortunately, the use of expensive flat Ti foil as a substrate seems to limit the maximal exposure of active sites as well as its scalable application due to the high cost. Carbon cloth (CC), an easily available and cheap carbon fiber, is highly conductive and flexible. Its use as electrode support bears the intrinsic benefits of low cost, robustness and self-standing 3D structure. Although 3D electrodes composed of WS_2 or MoS_2 nanoparticles on carbon cloth have been reported, there is no report on the directly growth of vertical aligned MoS_2 nanoplatelets on carbon cloth which is of great significance for practical application of water-splitting devices.

Herein, we demonstrate a simple way to fabricate vertically oriented MoS_2 and WS_2 nanosheet thin films grown on CC as efficient 3D electrodes for HER (detail available in the Supporting Information). Thanks to the nanostructured films composed of vertically aligned layers, resulting in large number of exposed active edges and timely repelling of as-formed H_2 bubbles, the well-designed 3D electrodes showed much higher electrochemical activities than flat MoS_2 and WS_2 nanosheet on CC.

Figure 1a&b show the low-magnification scanning electron microscopy (SEM) images of MoS_2/CC (a) and WS_2/CC (b), indicating the entire surface of the CC was uniformly covered with a layer of MoS_2/WS_2 nanosheet film. These films possessed a porous structure with only ~100 nm in depth (Figure S1, as indicated by the black arrows). The high-magnification SEM images (insets of Figure 1a&b) further reveal that such MoS_2/WS_2 nanosheets are vertically aligned on the CC surface, possessing a lateral size of around 200-300 nm. The corresponding energy dispersive X-ray (EDX) spectra (see Figure S2) suggest that the atomic ratio between Mo/W and S is close to 2:1. CC is a porous 3D electrode consisting of carbon fiber of 8 μm in diameter (see Figure S3). The highly textured surface of the carbon fiber facilities the nucleation and growth of a sulfide layer with strong mechanical interaction. It is noted that, after annealing at 350 ^oC for 2 h, the 2D nanosheet morphology is intact and the 3D porous architectures are well retained (Figure S4a&b). Figure1c&d are representative transmission electron microscopy (TEM) images of the MoS_2 and WS_2 nanosheet films, respectively, showing good agreement with SEM observation (Figure 1a&b). The light contrast in various areas of the TEM image indicates the thin two-dimensional (2D) nature. Moreover, the high-resolution (HR) TEM image (inset of Figure 1c) of the curled edge shows those MoS_2 nanosheets are composed of 7-10 layers (4-6 nm) with an interlayer spacing of 0.67 nm, while the WS_2 nanosheets show a thickness of ~ 10 nm with an interlayer distance of 0.62 nm (inset of Figure 1d), verifying the ultrathin nature of these vertically oriented MoS_2/WS_2 nanosheets. Figure 1e&f show the SEM images and the corresponding EDX elemental mapping images of the as-prepared MoS_2/CC and WS_2/CC electrodes, respectively, revealing that both Mo/W and S elements are uniformly distributed on the whole nanofiber.

To further characterize the chemical nature and bonding state of MoS_2/WS_2 on CC surfaces, X-ray photoelectron spectroscopy (XPS) was employed. As shown in Figure 2a, two characteristic peaks arising from Mo $3d_{5/2}$ and Mo $3d_{3/2}$ orbitals are located at 229.1 eV and 232.2 eV, suggesting the dominance of Mo (IV) in the freshly prepared MoS_2/CC product. Besides, small shoulder signals for Mo (VI) oxidation state are observed. In contrast, the Mo 3d spectrum of the annealed sample shows only a single doublet. Furthermore, the S $2p_{3/2\text{-}1/2}$ doublet peaks for the freshly prepared MoS_2 exhibit broader peaks at ~163 eV and 162 eV when compared with those of the annealed sample, indicating the existence of other binding signals, such as bridging S_2^{2-} or apical S^{2-}, which could result from the unsaturated S atoms and are known as active sites for HER.[19, 20] Thus better HER performance can be expected from the freshly-prepared S-rich MoS_2 sample.

Figure 2b shows the high-resolution XPS spectra of the W 4f and S 2p regions of the WS_2/CC products. For the WS_2/CC composite after annealing, black dotted lines have been added to bisect the W $4f_{7/2}$, W $4f_{5/2}$ and

W $5p_{3/2}$ peaks appeared at about 33.1eV, 35.2 eV and 38.7 eV, suggesting an oxidation state of W (IV), and the corresponding single doublet peaks for S $2p_{1/2}$ and $2p_{3/2}$ appeared at 162.4 eV and 163.6 eV, indicating the S^{2-}. These peaks in the annealed WS_2/CC are identical to those of highly crystalline WS_2.[21] For the freshly-obtained WS_2/CC, the doublet peaks of W 4f and S 2p were broader than those of the annealed WS_2/CC. Besides, a small negative shift about 0.5 eV was observed, which could be attributed to the adsorption of oxygen,[22] while the small shoulder observed at ~36 eV illustrates the existence of W (VI) at oxygen-rich environment as in WO_3.[23, 24] This indicates that the freshly-prepared WS_2/CC is more susceptible to oxidation.[25] It has been reported that WS_2 sample appear to be more susceptible to oxidation than MoS_2.[8]

For MoS_2 materials, the basal edges have been identified as the active sites for HER, but unfortunately, the overall conductivity of such materials is limited due to the poor electron transport among the domains and it thus reduces the total HER activity. In this work, the vertically oriented MoS_2/WS_2 nanosheet film grown on CC (a rough and curved surface) is expected to not only maximize the exposed active sites and overcome the limited electron/proton transport, but also accelerate the timely repelling of the as-formed bubbles by reducing the gas bubble adhesion due to the highly 'superaerophobic' surface.[12]

To verify our hypothesis, the HER performance of the 3D MoS_2/CC and WS_2/CC electrodes were demonstrated in 0.5 M H_2SO_4 solution using a three-electrode setup, where the electrode was tested in a static state without rotation to mimic real industrial operation. Electrochemical impedance spectroscopy (EIS) reveals similar system resistance (Rs, $2.5 \pm 0.3\Omega$) for all the tested electrodes (Figure S5). To exclude the influence of the series resistance from the system (Rs, such as wiring, solution and substrate), all of the data have been *i*R-corrected by subtracting the ohmic resistance loss form the overpotential. As control samples, flat MoS_2/CC and WS_2/CC film were also prepared and characterized by SEM (Figure S6) and XPS (Figure S7). As shown in Figure 3b, the cathodic polarization curve recorded for the nanostructured MoS_2/CC exhibited a low onset potential of ~0.1 V, which is much smaller than that of the flat MoS_2/CC and annealed MoS_2/CC and even lower than that of the reported Ti foil supported MoS_2 nanostructure.[13] As expected, our nanostructured MoS_2/CC electrode displays a highest current density among all the tested electrodes, 86 mA cm^{-2} at overpotential around -0.25 V. This is equivalent to ~450 mA mg^{-1} after normalized by the loading weight, which is almost two times larger than the value of the Ti foil supported MoS_2 nanostructure.[13] Since the cathodic current density is proportional to the amount of evolved hydrogen, the large current density here indicates prominent hydrogen evolution behavior of the vertically gowned

MoS_2/CC electrode. This may arise from the unique designed electrode structure which brings in more active sites along with the optimized conductivity and reduced gas bubble adhesion.

Interestingly, in the case of the WS_2/CC electrodes (Figure 3c), the annealed nanostructured WS_2/CC showed a highest current density (~15 mA cm^{-2}) among the tested WS_2 samples at the overpotential of -0.25 V. Although the annealed WS_2/CC electrode show lower activity than the nanostructured MoS_2/CC with 0.15 V larger overpotential to achieve cathodic current density of 86 mA cm^{-2}, it is still noteworthy because after normalized by the loading weight, this value (~15 mA cm^{-2} at -0.25 V) is about 7 times larger than that of carbon cloth supported WS_2 nanoparticles[23] and even slightly higher than that of WS_2/rGO.[26] This is likely due to the vertically oriented feature of our WS_2/CC electrode. It is noted that the annealed WS_2/CC electrode display much higher activity than the as-prepared WS_2/CC, this may be attributed to the removal of inactive impurities such as WO_3,[23] as verified by the XPS analysis.

The Tafel plots of these catalysts are shown in Figure 3d and are used to determine Tafel slopes and exchange current densities by fitting the Tafel plots to the equation of $\eta = b\log(j) + \log(j_0)$, where η is the overpotential, j the current density, j_0 the exchange current density, and b the Tafel slope.[27] The fitted Tafel plot for the nanostructured MoS_2/CC gives a b value of 50 mV/dec, which is much lower than that of the annealed MoS_2/CC and even slightly smaller than the recently reported value for pure MoS_2 nanoplates (53 mV/dec).[28] It is likely due to the oriented growth of MoS_2 nanosheets on CC which results in the improvement conductivity of the MoS_2 materials and the increase number of the exposed active sites. Then the exchange current density is determined to be 9.2×10^{-3} mA cm^{-2} for the nanostructured MoS_2/CC sample, almost one order of magnitude higher than the Ti foil supported MoS_2 nanostructure (3.87×10^{-4} mA cm^{-2})[13] and carbon fiber paper supported $MoSe_2$ (3.80×10^{-4} mA cm^{-2}).[18] Although the Tafel slope for annealed WS_2/CC is smaller than the freshly-prepared nanostructured WS_2/CC, this is still much higher than the MoS_2 and consistent with previous results.[23, 26] Moreover, these values compare favorably to most of the reported values for non-precious HER catalysts in acidic aqueous electrolytes (see Table S1 in the Supporting Information)

Stability is another important criterion used to evaluate a catalyst. A long-term cyclic voltammetry test was performed to assess the electrochemical stability of the nanostructured MoS_2/CC electrode in an acidic environment. As shown in Figure 4a, working under such condition, the nanostructured MoS_2/CC electrode and the annealed WS_2/CC electrode performed still steadily, suggested by the smooth curve recorded after 2000 cycles along with negligible current degradation. Furthermore, continuous chronoamperometric curve was also presented in Figure 4b, where a stable current density of ~22 mA cm^{-2} (at a overpotential of 0.2 V)

and ~17 mA cm^{-2} (at a overpotential of 0.25 V) over an operating period of 24 h were observed for the nanostructured MoS_2/CC and annealed WS_2/CC, respectively, further revealing the high stability of these nanostructured electrodes. Although, for a practical electrode device, the stability performance will need to be maintained much longer time, the performance of as-prepared electrodes in this work show great potential for scalable application. Notably, our MoS_2/CC and WS_2/CC electrodes are robust enough to withstand an ultrasonication even for 30 min (Figure S8), indicating the strong binding between the CC and the nanostructured MoS_2 /WS_2 sheets, which ensures the excellent stability of those nanostructured electrodes. Notably, it is observed that the small H_2 bubbles formed on the 3D electrode can be timely released during the working process, which in turn ensures sufficient number of active sites, resulting in a stable electrocatalytic performance (details can be seen in SI-2). This is fully consistent with the previous observation.[13]

As discussed above, such high catalytic performance of the nanostructured MoS_2/WS_2 electrodes could be due to following reasons: (1) The intimate contact of MoS_2 and WS_2 nanosheets with CC enables good mechanical binding and electrical connection, facilitating the flow of electrons from CC to MoS_2 or WS_2 nanosheet arrays during HER. This is of great significance for the semi-conductive catalysts such as MoS_2 and WS_2. (2) The 3D configurations of the vertically oriented MoS_2/CC and WS_2/CC electrodes not only facilitate the self-removal of as-formed H_2 bubbles form the nano-porous electrode surfaces, but also ensure enough and open spaces which allows easy diffusion of electrolyte into all the active sites and thus more efficient use of the entire electrode. (3) The ultrathin MoS_2/WS_2 vertical nanosheets could be a better structure compared to the multilayer nanoparticles because electrons only need to be transferred from the support to the platelets, instead of passing through different layers. (4) The vertically oriented S-rich MoS_2 nanosheet arrays and the annealed WS_2 nanosheets with low oxidized species expose more active sites for HER than those of flat ones.

In summary, we developed a simple solvothermal method to fabricate MoS_2 and WS_2 grown on CC electrodes with vertically oriented nanosheet layers. With the unique layer orientation that maximally exposes the active edge sites as well as a rapid release of small gas bubbles to provide constant working electrode area, the nanostructured MoS_2/CC electrode exhibits excellent HER activity, while the WS_2/CC catalyst is also investigated here as a novel active HER architecture for potential use as HER catalyst. Both materials exhibit prominent electrochemical durability thanks to the strong bonding between the nanosheet layers and the substrate along with the self-removal of the as-formed H_2 bubbles from the nano-porous electrode surface. Moreover, these vertically oriented layered catalysts can be readily applied in diverse

water electrolysis devices as easily-available, high-performance and stable HER catalysts.

Acknowledgment

This project is funded by the National Research Foundation (NRF), Prime Minister's Office, Singapore under its Campus for Research Excellence and Technological Enterprise (CREATE) programme. We also acknowledge financial support from the academic research fund AcRF tier 1 (M4011020 RG8/12 and M4011253 RG 7/14) Ministry of Education, Singapore.

Electronic supplementary information (ESI) available: Experimental section and figures. See DOI:

References

1. J. A. Turner, *Science*, 2004, **305**, 972-974.
2. J. N. Armor, *Catal. Lett.*, 2005, **101**, 131-135.
3. M. G. Walter, E. L. Warren, J. R. McKone, S. W. Boettcher, Q. Mi, E. A. Santori and N. S. Lewis, *Chem. rev.*, 2010, **110**, 6446-6473.
4. M.-R. Gao, Y.-F. Xu, J. Jiang and S.-H. Yu, *Chem. Soc. Rev.*, 2013, **42**, 2986-3017.
5. A. B. Laursen, S. Kegnaes, S. Dahl and I. Chorkendorff, *Energy Environ. Sci.*, 2012, **5**, 5577-5591.
6. M. Chhowalla, H. S. Shin, G. Eda, L.-J. Li, K. P. Loh and H. Zhang, *Nat. Chem.*, 2013, **5**, 263–275.
7. Y. Yan, B. Xia, X. Qi, H. Wang, R. Xu, J.-Y. Wang, H. Zhang and X. Wang, *Chem. Commun.*, 2013, **49**, 4884-4886.
8. M. A. Lukowski, A. S. Daniel, C. R. English, F. Meng, A. Forticaux, R. J. Hamers and S. Jin, *Energy Environ. Sci.*, 2014, **7**, 2608-2613.
9. D. Voiry, H. Yamaguchi, J. Li, R. Silva, D. C. B. Alves, T. Fujita, M. Chen, T. Asefa, V. B. Shenoy, G. Eda and M. Chhowalla, *Nat. Mater.*, 2013, **12**, 850-855.
10. J. Lin, Z. Peng, G. Wang, D. Zakhidov, E. Larios, M. J. Yacaman and J. M. Tour, *Adv. Energy Mater.*, 2014, **4**, DOI: 10.1002/aenm.201301875.
11. Z. Wu, B. Fang, A. Bonakdarpour, A. Sun, D. P. Wilkinson and D. Wang, *Appl. Catal. B*, 2012, **125**, 59-66.
12. T. F. Jaramillo, K. P. Jørgensen, J. Bonde, J. H. Nielsen, S. Horch and I. Chorkendorff, *Science*, 2007, **317**, 100-102.
13. Z. Lu, W. Zhu, X. Yu, H. Zhang, Y. Li, X. Sun, X. Wang, H. Wang, J. Wang, J. Luo, X. Lei and L. Jiang, *Adv. Mater.*, 2014, **26**, 2683-2687.
14. Y. Yan, B. Xia, Z. Xu and X. Wang, *ACS Catal.*, 2014, 1693-1705.
15. Y. H. Chang, F. Y. Wu, T. Y. Chen, C. L. Hsu, C. H. Chen, F. Wiryo, K. H. Wei, C. Y. Chiang and L. J. Li, *Small*, 2013, DOI: 10.1002/smll.201302407.
16. P. D. Tran, S. S. Pramana, V. S. Kale, M. Nguyen, S. Y. Chiam, S. K. Batabyal, L. H. Wong, J. Barber and J. Loo, *Chem.- Eur. J.*, 2012, **18**, 13994-13999.
17. D. Kong, H. Wang, J. J. Cha, M. Pasta, K. J. Koski, J. Yao and Y. Cui, *Nano lett.*, 2013, **13**, 1341-1347.
18. H. Wang, D. Kong, P. Johanes, J. J. Cha, G. Zheng, K. Yan, N. Liu and Y. Cui, *Nano Lett.*, 2013, **13**, 3426-3433.
19. D. Merki, S. Fierro, H. Vrubel and X. L. Hu, *Chem. Sci.*, 2011, **2**, 1262-1267.

20. D. Li, U. Maiti, J. Lim, D. S. Choi, W. J. Lee, Y. Oh, G. Y. Lee and S. O. Kim, *Nano lett.*, 2014.
21. R. Morrish, T. Haak and C. A. Wolden, *Chem. Mater.*, 2014, **26**, 3986-3992.
22. I. Martin, P. Vinatier, A. Levasseur, J. C. Dupin and D. Gonbeau, *J. Power Sources*, 1999, **81–82**, 306-311.
23. T.-Y. Chen, Y.-H. Chang, C.-L. Hsu, K.-H. Wei, C.-Y. Chiang and L.-J. Li, *Int. J. Hydrogen Energy*, 2013, **38**, 12302-12309.
24. A. Benadda, A. Katrib, J. W. Sobczak and A. Barama, *Appl. Catal. A*, 2004, **260**, 175-183.
25. B. K. Miremadi and S. R. Morrison, *J. Appl. Phys.*, 1988, **63**, 4970-4974.
26. J. Yang, D. Voiry, S. J. Ahn, D. Kang, A. Y. Kim, M. Chhowalla and H. S. Shin, *Angew. Chem. Int. Ed.*, 2013, **52**, 13751-13754.
27. J. O. M. Bockris and E. C. Potter, *J. Electrochem. Soc.*, 1952, **99**, 169-186.
28. Y. Yan, B. Xia, X. Ge, Z. Liu, J.-Y. Wang and X. Wang, *ACS Appl. Mater. Interfaces*, 2013, **5**, 12794-12798.

Figures and Captions

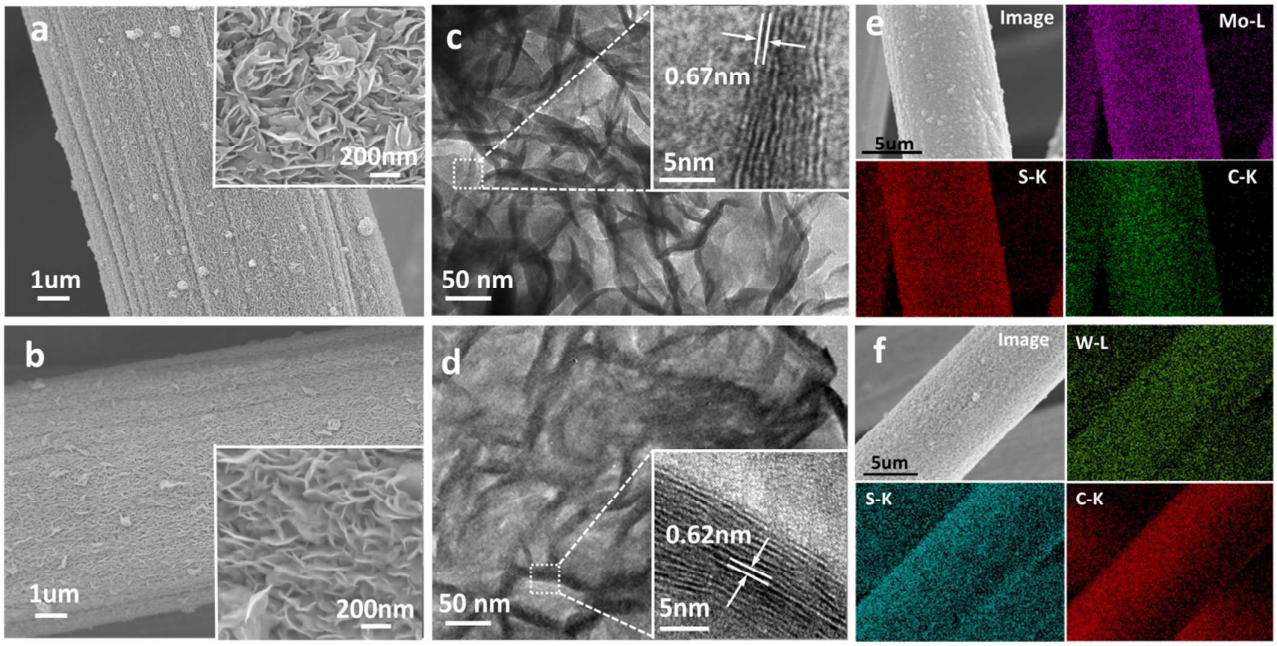

Figure 1. (a, b) Low and high-magnification (insets) SEM images of nanostructured MoS_2/CC electrode (a) and WS_2/CC electrode (b). (c, d) TEM and high-resolution (HR) TEM (insets) images of nanostructured MoS_2/CC electrode (c) and WS_2/CC electrode (d). (e, f) The corresponding SEM image and EDX elemental mapping of Mo, S and C for the nanostructured MoS_2/CC electrode (c) and W, S and C for WS_2/CC electrode (d).

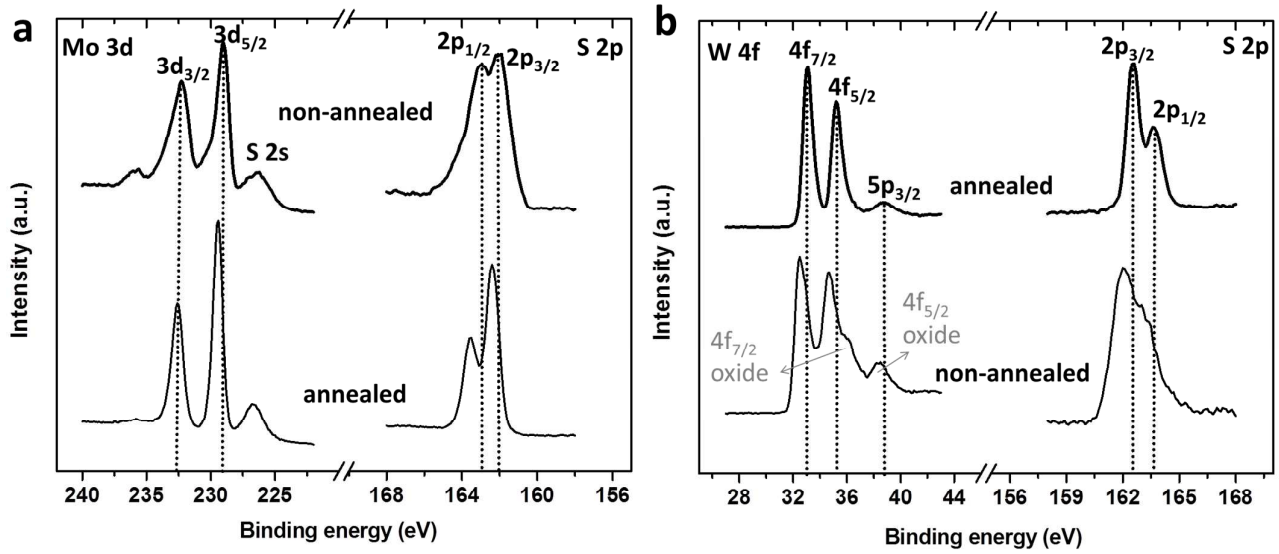

Figure 2. XPS spectra of Mo 3d and S 2p in the MoS_2/CC sample (a) and W 4f and S 2p in the WS_2/CC sample (b), as-synthesized and after thermally annealed at 350 °C.

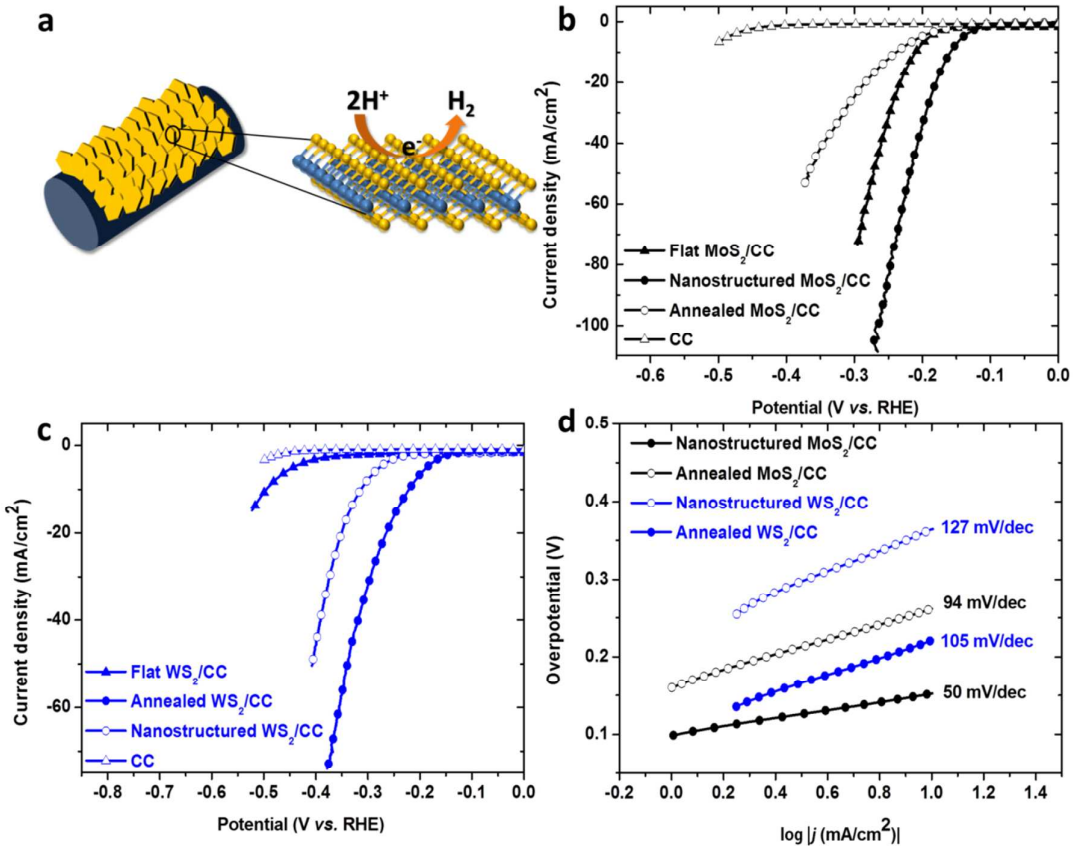

Figure 3. (a) Schematic illustration of nanostructured MoS_2/CC and WS_2/CC electrodes. The active Mo/W edge for HER is marked in the magnified crystal structure image. Blue sphere: Mo/W; yellow sphere: S. Polarization curves (after *i*R-correction) of MoS_2/CC (b) and WS_2/CC catalysts (c). (d) The corresponding Tafel plots of the samples.

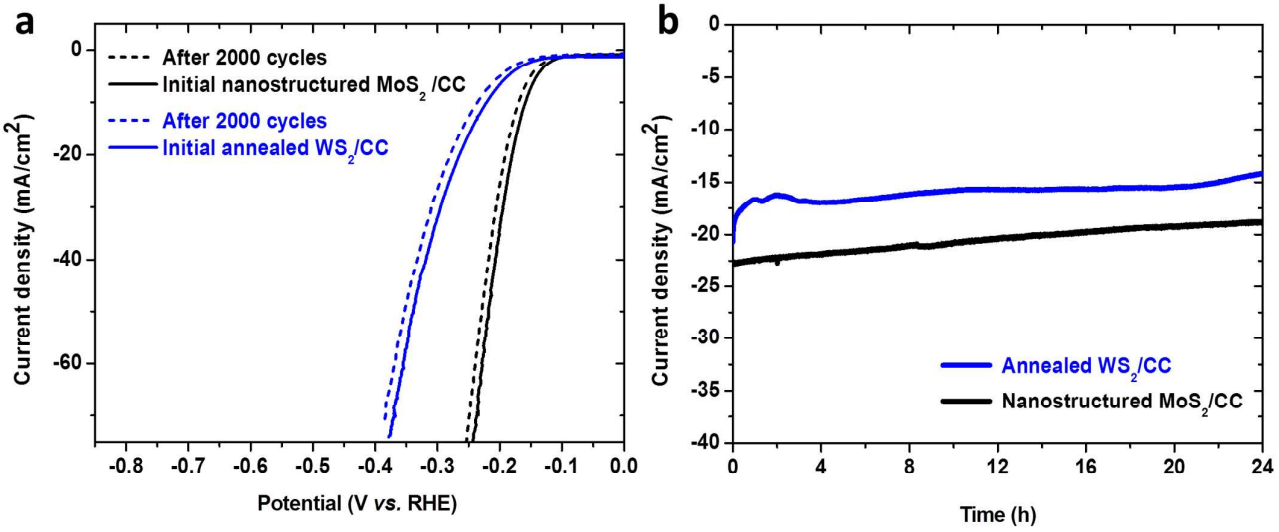

Figure 4. Stability testing of the nanostructured MoS_2/CC electrode and annealed WS_2/CC electrode. (a) Polarization curves of the electrodes before and after 2000 CV scans between +0.1 and −0.5 V vs. RHE. (b) Chronoamperometric curve for both electrodes under static overpotential of 200 mV and 250 mV for 24 h, respectively.

A table of contents entry

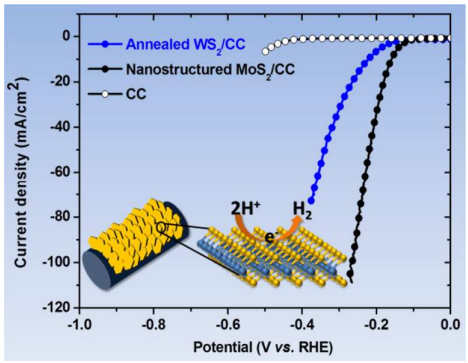

Vertically oriented MoS_2 and WS_2 nanosheet thin films grown on CC have been designed as efficient 3D electrodes for hydrogen evolution reaction.